RSC Advances

PAPER

View Article Online
View Journal | View Issue

Open Access Article. Published on 18 February 2020. Downloaded on 1/20/2026 11:38:05 AM.
This article is licensed under a Creative Commons Attribution-NonCommercial 3.0 Unported Licence.

Check for updates

Cite this: *RSC Adv.*, 2020, **10**, 7377

A high rectification ratio nanofluidic diode induced by an "ion pool"†

Qingqing Liu,[a] You Liu,[a] Bingxin Lu,[a] Yuting Wang,[a] Yanglei Xu,[b] Jin Zhai *[a] and Xia Fan *[a]

Inspired by functionalized biological ion channels, artificial channels were prepared to mimic the natural ones. The key concept behind the rectifying phenomena in nanochannels is the construction of asymmetric restrictive nanochannels. Here, we prepared nanoporous oxidized polyvinyl alcohol (PVA) and WO_3 composite coatings on hourglass-shaped anodic aluminum oxide (AAO) nanochannel surfaces. Accordingly, a special "ion pool" is formed between the homogeneous junction in the middle of the AAO and the nanoporous PVA/WO_3 film-covered AAO surface and its two ends are greatly nano-confined. Ion enrichment and ion depletion occur in the "ion pool" and are dependant on the applied voltage polarity. A rectification ratio of 458, which is in accordance with the highest value found in previous reports, was obtained from the cooperative effects of the two small open ends of the "ion pool". Furthermore, this value is enhanced to about 2000 under constant voltage. An excellent pH-sensitive rectification property, with a single rectification direction from acidic to basic conditions, has also been demonstrated.

Received 1st November 2019
Accepted 6th January 2020

DOI: 10.1039/c9ra09006a

rsc.li/rsc-advances

Introduction

Various biological ion channels or biological semipermeable membranes play important roles in cell material exchange, signal transduction, energy conversion *etc.*[1,2] Inspired by the structure and function of protein channels, researchers began to prepare artificial nanochannels to mimic natural channels for biosensing, energy conversion, and smart gating.[3–6] Organic polyethylene terephthalate (PET) conical channels and inorganic AAO nanochannel arrays are the most widely studied.[7–12] Until now, one of the most important discoveries in the field of electrolyte ion transport by artificial solid nanochannels is the unidirectional ion rectification characteristics that originate from asymmetric systems.[13–15] However, artificial channels still have many deficiencies compared with the highly functionalized ion channels in living organisms. For example, artificial PET channels were prepared *via* an expensive track etching method.[16–18] The sizes of the ion channels in nature are usually similar to that of the ions or molecules that are being transported, while the diameters of AAO channels are usually dozens of nanometers.[9–12,19] Other types of nanochannels, such as nanofluidic crystals, are densely packed nanoparticles produced by numerous interconnected three-dimensional gaps that form nanochannels.[20–22] New types of dynamic curvature nanochannels have also been made such as dynamic curvature nanochannels.[23] Each type of nanochannel has its own unique characteristics due to their respective structural features.[24,25]

In recent years, the preparation of heterogeneous structures on AAO surfaces has become a research hotspot in the field of artificial ion channels because the asymmetric structure may produce new functions. Mesoporous carbon, anatase TiO_2, amphiphilic block copolymers, and many other functional materials have been used in combination with the AAO nanochannels.[26–32] The asymmetric structure and charge distribution produce a strong ion rectifying effect and rectification ratios of up to 449 and 489 were obtained in AAO nanochannels combined with mesoporous carbon or an amphiphilic block copolymer, respectively.[26,30] However, in these asymmetric nanochannel structures, ionic and molecular transport is only governed by one or two tip sides and ion enrichment and depletion are induced by a polar surface charge in the confined symmetric space.

The key concept of rectifying phenomena in nanofluids is that the construction of asymmetric structure or asymmetric surface charge distribution with nano-confined restrictive channels.[33] Inspired by this, we creatively designed heterogeneous nanochannels of nanoporous PVA/WO_3 composite

[a]*Beijing Key Laboratory of Bio-Inspired Energy Materials and Devices, School of Chemistry, Beihang University, Beijing 100191, P. R. China. E-mail: zhaijin@buaa.edu.cn*

[b]*Beijing Key Laboratory of Lignocellulosic Chemistry, College of Materials Science and Technology, Beijing Forestry University, Beijing 100083, P.R. China. E-mail: xuyanglei@bjfu.edu.cn*

† Electronic supplementary information (ESI) available: SEM image of the middle region of the hourglass-shaped AAO; SEM of the cross section of the oxidized PVA modified hourglass-shaped AAO openings; histogram of rectification ratio calculated from the *I–V* curves of AAO-PVA in different KCl concentration. See DOI: 10.1039/c9ra09006a

Open Access Article. Published on 18 February 2020. Downloaded on 1/20/2026 11:38:05 AM.
This article is licensed under a Creative Commons Attribution-NonCommercial 3.0 Unported Licence.

coatings and covered hourglass-shaped AAO *via* a facile spin coating method. The heterogeneous junction greatly reduced the opening size of the surface nanochannels, while the homogeneous junction in the middle region also greatly reduced the size of the AAO channels. A special "ion pool" with long dimensionality is formed between the two junctions with both ends being greatly nano-confined. Compared with the previous reports on heterogeneous nanochannels, this study not only forms an asymmetric structure, chemical components, and surface charge distribution but also greatly enhances the nano-confined effect. Ionic selective transportation control across the "ion pool" depends on the cooperative effect of the two small open ends and the long nano-confined pathway, which can dramatically enhance the ion enrichment and ion depletion performance of the system, leading to a high rectification ratio of 458. Furthermore, this value is greatly enhanced to about 2000 under the constant voltage. Also, an excellent pH-sensitive rectification property, with a single rectification direction from acidic to basic conditions, has been demonstrated because the components have different isoelectric points. This concept of making additional nano-confined interspaces on the basis of the existing nanochannels has great potential for the preparation of advanced functional nanomaterials.

Experimental section

Fabrication of the symmetric hourglass-shaped AAO nanochannels

The symmetric hourglass-shaped AAO nanochannels were fabricated using the two step anodization method combined with an *in situ* pore opening process. An aluminium foil of 0.1 mm in thickness was used as the anode, while a stainless plate was used as the counter electrode in the anodization process. First, a clean foil was electrically polished in a mixed solution of $HClO_4$ and ethanol (1 : 4 in volume ratio) under a DC voltage of 17 V at 0–5 °C. Then, the foil was anodized for 2 h in a 0.3 mol L^{-1} oxalic acid solution under a DC voltage of 50 V at 0–5 °C as the first anodization process. The foil was then exposed to an aqueous solution of phosphoric acid (6 wt%) and chromic acid (3.5 wt%) at 90 °C for 1 h. The second anodization process was conducted under the same conditions as the first anodization process until the anodized current decreased to 0 A. Finally, an *in situ* pore opening procedure was performed for 30 min to form symmetric hourglass-shaped alumina nanochannels.[11]

Fabrication of the asymmetric rectifying system

First, 0.36 g of polyvinyl alcohol (MW = 22 000) was fully dissolved in a 5 mL water and 5 mL ethanol mixed solution at 70 °C. PVA-modified hourglass-shaped AAO was prepared *via* spin coating the former solution on one side of the blank hourglass-shaped AAO at 3000 rpm for 20 seconds. For the AAO-PVA/WO_3 sample, 0.64 g of WO_3 nanoparticles (Aladdin) with an average diameter of 50 nm were added to the former solution, followed by mechanical agitation and ultrasonication for 20 minutes each. This dispersal process was conducted three times. After standing for 12 hours, the upper suspension was used for spin coating. All samples were heat-treated at 300 °C for 30 min in a muffle furnace at a heating rate of 3 °C min^{-1}. After natural cooling, these samples were used for characterization and ion current measurements.

Characterization

Surface and cross-sectional images of the hourglass-shaped AAO and the oxidized PVA or PVA/WO_3 covered hourglass-shaped AAO were characterized *via* a JSM 7500F scanning electron microscope (SEM).

Ion current measurements

The ion transport characteristics of the hourglass-shaped AAO and the oxidized PVA or PVA/WO_3 covered hourglass-shaped AAO were characterized by measuring the ion current. The electrolyte was a KCl (Beijing Chemical Factory) aqueous solution of different concentrations. Ion current was measured using a Keithley 6487 picoammeter (Keithley Instruments, Cleveland, OH). Two Ag/AgCl electrodes were used as the electrodes for apply voltage and conducting ion current because of their good stability and high sensitivity. The unmodified side of the hourglass-shaped AAO was always facing the negative electrode. *I–V* curves were recorded with a transmembrane voltage varying from −2 V to +2 V. KCl solutions with different pH values were adjusted using HCl or KOH. For constant voltage mode measurements, the voltage was fixed at +2 V or −2 V.

Results and discussion

Characterization studies

Anodized alumina is one of the most important materials that has been widely studied for constructing a variety of smart artificial nanochannel systems. Herein, we selected a special structural anodic alumina channel, namely hourglass-shaped AAO as the substrate supporter, which provided the desired transmembrane environment and possesses a very narrow tip channel that is localized inside the nanochannels to effectively control the ion transport.[11,12] As shown in Scheme 1a, the AAO-PVA/WO_3 heterogeneous structure was prepared by spin coating a mixed solution, containing the WO_3 nanoparticles, PVA, water, and ethanol onto one side of the hourglass-shaped AAO nanochannels. This was followed by 30 minutes of heat-treatment at 300 °C for the moderate oxidation of PVA and immobilization of WO_3 nanoparticles onto the surface of the AAO nanochannels. From the SEM images in Scheme 1b–d confirmed that PVA/WO_3 was successfully immobilized onto the surface of the hourglass-shaped AAO. PVA is a commercialized organic chain material with hydroxyl groups and it can increase the dispersion of WO_3 nanoparticles in a solvent, thus making the coating more uniform during the spin coating process. As seen in the photograph of a PVA/WO_3-covered hourglass-shaped AAO in Fig. S1,† the surface of the AAO turns yellow in color after heat treatment. This simple heat treatment moderately oxidized the PVA, which greatly reduced the number of hydroxyl groups in the PVA and

Open Access Article. Published on 18 February 2020. Downloaded on 1/20/2026 11:38:05 AM.
This article is licensed under a Creative Commons Attribution-NonCommercial 3.0 Unported Licence.

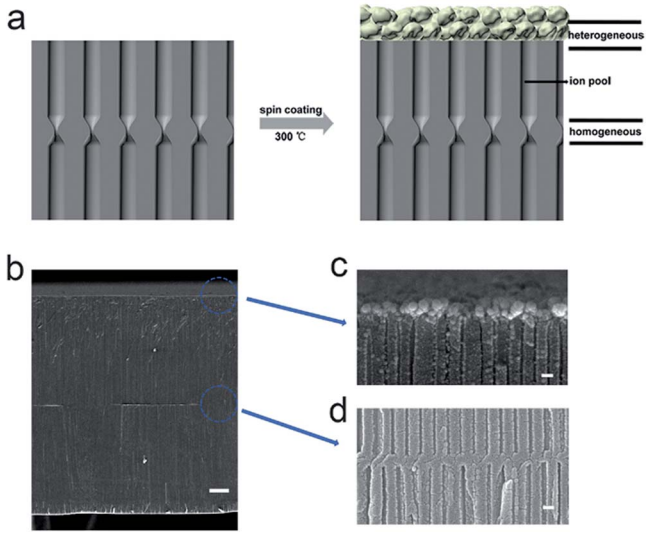

Scheme 1 (a) A flow chart of the facile fabrication of AAO-PVA/WO_3 nanochannels. The nanoparticles aggregate onto the channel surfaces represent the nanoporous PVA/WO_3 surface coating. (b) SEM image of a cross-section of the as-prepared PVA/WO_3-AAO, the sale bar is 10 μm. (c) SEM image of the surface heterojunction, the scale bar is 100 nm. (d) SEM image of the middle homogeneous junction of the hourglass-shaped AAO, the scale bar is 100 nm.

prevented the dissolution of the PVA/WO_3 coating in the aqueous solution. Finally, PVA also enhanced the stability of the AAO-PVA/WO_3 nanochannels during the subsequent ion transport investigations.

As is shown in Fig. 1(a), the average pore diameter of the hourglass-shaped AAO surface was determined to be 30–40 nm, while the thickness of the hourglass-shaped AAO is 90–110 microns. From Fig. 1(b), we can see that the opening of the AAO nanochannel surfaces covered with oxidized PVA is slightly blocked to a certain extent but the PVA does not make a complete film on the surface. Further, a thin nanoporous structure consisting of PVA/WO_3 nanoparticles is formed on the surface of the hourglass-shaped AAO, forming the heterogeneous AAO-PVA/WO_3 nanochannels, as shown in Fig. 1(c) and (d). Here, the oxidized PVA connects the WO_3 nanoparticles and the AAO surface together to form a thin coating with a thickness of only about 100–150 nm. Compared with oxidized PVA-modified AAO nanochannel surfaces, the openings of the PVA/WO_3 nanoparticle-coated AAO surfaces are more clogged. Due to the irregular shape of the nanoparticles, small gaps exist between adjacent nanoparticles, which form the nanochannels for ion transport.

Ion transport characteristic of the asymmetric system

Ion current rectification is one of the key parameters in the study of artificial ion channels.[34–38] Typically, ion current rectification can be realized by channels with asymmetric surface charges, structures or electrolyte concentrations.[39,40] In order to realize the asymmetry of the channel, previous reports mainly focused on the various modifications of the inner surface of the channels.[41–46] Here, oxidized PVA and the thin nanoporous PVA/WO_3 film decorated hourglass-shaped AAO nanochannels also make the whole channel structure asymmetric. In order to fully study the ion transport properties of the asymmetric structure, ionic current–voltage curves (*I–V*) were measured under different KCl concentrations and pH values and at a constant voltage maintained with Ag/AgCl electrodes.

The *I–V* curve of the blank hourglass-shaped AAO in a 10 mM KCl solution is linear, as shown in Fig. 2(a), while the AAO modified with oxidized PVA or PVA/WO_3 shows significant rectification. In general, the rectification ratio is defined as the absolute value of the current ratio at +2 V and −2 V. Here, as the structure of the hourglass-shaped AAO is completely symmetrical, it exhibits non-rectifying properties, while the rectification ratio of the oxidized PVA-modified AAO in a 10 mM KCl solution is 9.8. When the hourglass-shaped AAO nanochannels were completely covered *via* a nanoporous PVA/WO_3 thin film, the ionic current at −2 V is just −5.13 nA and the ionic current is 2.35 μA at +2 V, so the rectification ratio reached 458, which is similar to the highest value reported in the field of nanofluid rectification.[29] Thus, these heterogeneous nanochannels can be used as one of the candidates for the future practical applications as diodes in electronic circuits because the fabrication method is very simple and the cost of production is very low. As the nanochannels have the channel size in the nanoscale, the concentration of the electrolyte has an obvious influence on the ionic conductivity.[29,47–49] As is shown in Fig. 2(c), the conductance of the naked hourglass-shaped AAO, modified with oxidized PVA or a PVA/WO_3 thin film in a 0.1 M KCl solution, is

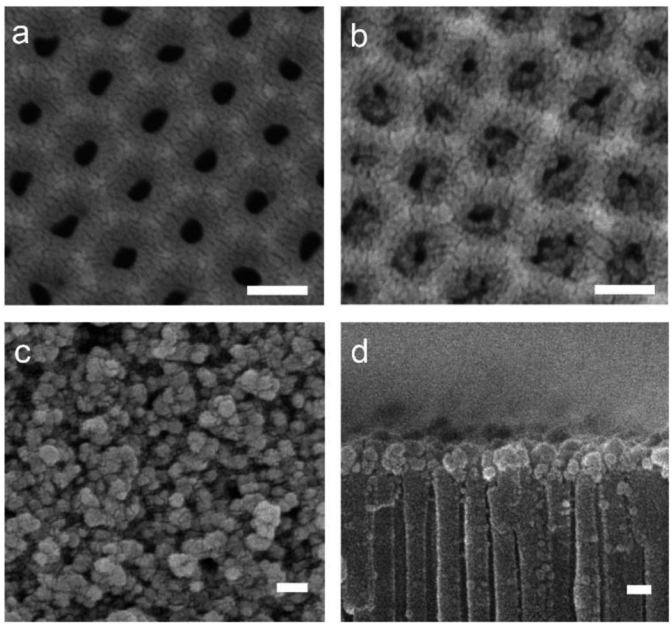

Fig. 1 SEM images. (a) Surface of the AAO nanochannels. (b) Surface of the PVA-modified AAO nanochannels. The opening of the nanochannels were slightly blocked. (c) Surface of the PVA/WO_3 covered AAO nanochannels, showing that nanoporous structures were formed. (d) A cross-section of the PVA/WO_3 coating, showing that the opening of the nanochannels are covered with WO_3 nanoparticles immobilized by oxidized PVA. The scale bar is 100 nm.

Open Access Article. Published on 18 February 2020. Downloaded on 1/20/2026 11:38:05 AM.
This article is licensed under a Creative Commons Attribution-NonCommercial 3.0 Unported Licence.

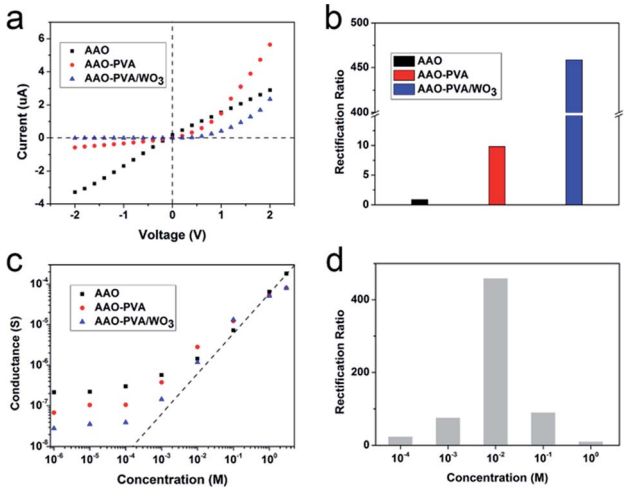

Fig. 2 Characterization of the ionic rectification. (a) I–V curve of the hourglass AAO, AAO-PVA, and AAO-PVA/WO_3 measured in a 10 mM KCl solution under neutral conditions. (b) Histogram of the rectification ratio calculated from the I–V curves of (a). (c) The ionic conductance of hourglass AAO, AAO-PVA, and AAO-PVA/WO_3 at different KCl concentrations. The dashed line is the conductance of the bulk solution. (d) The rectification ratios of AAO-PVA/WO_3 at different KCl concentrations.

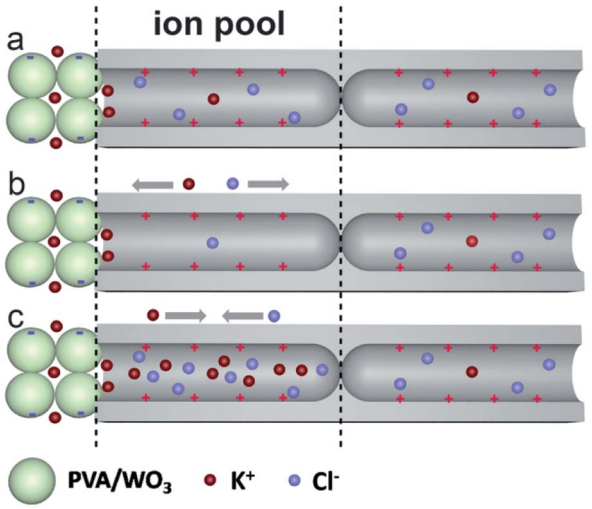

Scheme 2 Mechanism diagram of the rectifying effect under neutral condition of the PVA/WO_3 covered hourglass-shaped AAO. The "ion pool" is between the dashed line. (a) The equilibrium states. (b) Ion depletion state: when a negative bias is applied, both K^+ and Cl^- would migrate to the external solution. (c) Ion enrichment state, when a positive bias is applied, both K^+ and Cl^- would migrate to the "ion pool" area.

much higher than that of the bulk solution, which is one of the characteristics of nanochannels, including one-dimensional and two-dimensional nanochannels, and three-dimensional porous channels.[29,50–54] This phenomenon arises from ion transportation controlled by the surface charge of the channels and it also has a significant influence on ion rectification. The rectification ratios of the PVA/WO_3 thin film-modified hourglass-shaped AAO nanochannels under different KCl concentrations are shown in Fig. 2(d) and the maximum rectification ratio is at a 10 mM KCl solution. The rectification ratios decreased at other concentration conditions. This phenomenon is consistent with previous theoretical and experimental reports that state that a rectifying system usually has the highest rectification ratio at a certain concentration.[29,35–38]

The ion enrichment and depletion effects of nanochannel structures are considered the most important mechanisms for ion rectification in artificial ion channels.[13,47,49] They can also be used to explain the rectifying phenomenon in this study. The nanochannels have a great influence on ion transport due to the small channel size that is dependent on the tip region of the hourglass-shaped AAO and the gap channel within the nanoporous PVA/WO_3 film. The PVA/WO_3-modified hourglass-shaped AAO has a heterogeneous structure, where the main asymmetrical functional part is half of the hourglass-shaped AAO. One end can be seen as a homogenous Al_2O_3 junction with extremely small nanochannels, while the other end can be seen as a thin nanoporous PVA/WO_3 layer covered with AAO nanochannels, as shown in Scheme 2. Half of the AAO nanochannels with lengths between 45–55 microns can be seen as the "ion pool". When the surface of a nanochannel is positively or negatively charged, it tends to be more favorable for the transport of ions with the opposite charge.[55,56] The isoelectric point of alumina oxide is located at 8–9, so its surface is positively charged under acidic or neutral conditions, which means it tends to transport negatively charged Cl^- ions.[36] On the contrary, the moderate oxidation of PVA results in carbonyl groups on the surface, thus the adsorption of hydroxyl ions on the surface makes it negatively charged under neutral and alkaline conditions. Also, the isoelectric point of WO_3 is located at 0–1, it also tends to be negatively charged under neutral and alkaline conditions. As a result, when both ends of the AAO-PVA/WO_3 nanochannels are in a KCl solution of pH 7, oppositely charged ion enrichment occurs on the nanochannel inner surface. K^+ ions stay on the PVA/WO_3 side, while Cl^- ions are located on the hourglass-shaped AAO side. This equilibrium state will be broken when an external voltage is applied to the system. As is shown in Scheme 2b, when a negative voltage is applied to the system, both Cl^- and K^+ ions will migrate from the "ion pool" to the external solution, leading to ion depletion in the "ion pool" between the homogenous junction of the hourglass-shaped AAO and the heterogeneous junction of the PVA/WO_3 film covered AAO opening. The ion conductivity decreases due to ion depletion, as shown in the I–V curves of which the current under negative voltage is very small. On the contrary, when the voltage is reversed, the surface enriched ions, Cl^- and K^+, both migrate into the "ion pool" across the two junctions, thus causing ion enrichment in the "ion pool" area, as is shown in Scheme 2c. The ion enrichment greatly enhanced the conductance of the "ion pool", which is reflected in the I–V curves where the current is relatively high under a positive voltage. Ionic selective transportation across the "ion pool" depends on the cooperative effect of the two small open ends and the long nano-confined pathway of the "ion pool". Moreover, the dramatically enhanced ion enrichment and ion

Open Access Article. Published on 18 February 2020. Downloaded on 1/20/2026 11:38:05 AM.
This article is licensed under a Creative Commons Attribution-NonCommercial 3.0 Unported Licence.

depletion performance lead to the observed high rectification ratio.

In aqueous solutions, the surface electricity of a metal oxide or an oxygen atom rich surface is related to the pH value due to the adsorption or desorption of protons or hydroxide ions.[43,57,58] The *I–V* curves of the PVA/WO_3 covered hourglass-shaped AAO nanochannels were measured under different pH conditions in a 10 mM KCl solution, as shown in Fig. 3(a). Here, solutions at pH 3, pH 7, and pH 11 represent acidic, neutral and alkaline conditions, respectively. The rectification ratio shows the highest value under neutral solution, and the rectification ratio is greatly reduced at pH 3, as is shown in Fig. 3(b). The isoelectric points of the components are different under neutral conditions, the AAO side is positively charged, while the PVA/WO_3 side is negatively charged. This asymmetric structure and surface charge distribution results in the high rectification ratio. Under acidic conditions, the surface of the PVA/WO_3 side is almost electrically neutral, which lowers the selective enrichment of the ions, thus the asymmetry of the system is greatly reduced, resulting in the lowest rectification effect. Under alkaline conditions, the active sites of the PVA/WO_3 surface are all activated with a high negative charge density, which results in the maximum ion current under a positive voltage when compared to either acidic or neutral conditions. However, the rectification ratio of the system under alkaline conditions decreased because the surface of the AAO side is also negatively charged, which would reduce the asymmetric charge distribution in the system. The surface charge conditions are shown in Scheme S1.† Overall, sensitivity across a wide-range of pH values is observed in this study, of which a single rectification direction is activated from acidic to basic conditions. This result is similar to our previously reported organic/inorganic hybrid nanochannels.[59] However, simultaneously, a higher pH selectivity is first developed in this work because the maximum rectification ratio occurred at the opposite surface charge state, which shows a better coupling effect.

The rectified *I–V* curve of the ion channels is usually compared to the curve of the semiconductor diode in an integrated circuit. These two structures represent the rectifying of the electrons and ions; however, the volume of the ions in the solution is much larger than that of the electron in the solid. The concentration of ions within the enrichment and depletion areas varies with the applied voltage in the *I–V* test and the ion enrichment and depletion processes require time. Here, in order to better prove that the "ion pool" strategy plays a vital role in the high rectifying property of our as-prepared AAO-PVA/WO_3 nanochannels, we used the constant voltage mode of the picoammeter to measure the change in ion current. In this case, ion enrichment and ion depletion increased with time. As shown in Fig. 4, under constant voltage, the ion current of the oxidized PVA-modified AAO nanochannels at +2 V gradually increased from 5.3 μA to 8.5 μA, while the ion current at −2 V gradually decreased to −0.36 μA. The corresponding rectification ratio increased from 9.1 to 23.8. For the PVA/WO_3 covered AAO nanochannels, the ion current at +2 V gradually increased from 2.1 μA to 5 μA, while the ion current at −2 V gradually decreased to just −2.65 nA, thus producing a rectification ratio of about 1900–2000. At a constant voltage, the rectification ratio is about 4 times larger than the rectification ratio obtained using a scanning voltage from −2 V to +2 V. Compared with the data of the *I–V* curve in the fast scanning from −2 V to +2 V, we think that this enhanced rectification ratio comes from the longer response times of the ion enrichment and depletion under the constant voltage mode, which was caused by the "ion pool" structure with long dimensionality in our fabricated heterogeneous nanochannels. The special ends of the "ion pool" produce a large reduction in the opening area of the channels and results in a strong ion transport restrictive effect. That is, under a negative constant voltage, the ions would be continuously removed from the "ion pool" without being supplemented by the external solution, which results in a gradual decrease in the conductance, as is reflected by the gradually decreased in the ion current. When it comes to the positive constant voltage, both Cl^- and K^+ would be continuously transported to the "ion pool", causing an increase in conductance, as is reflected in the gradually increasing ion current in Fig. 4. It is important to note that the increase in the rectification ratio under constant voltage is larger than that of the PVA modified AAO nanochannels, probably because the plugged openings in the nanoporous PVA/WO_3 cause a more nano-confined "ion pool", producing stronger restrictions on ion transport and a more noticeable enhancement of rectification.

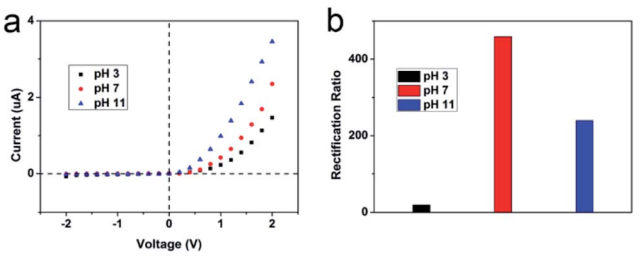

Fig. 3 Characterization of the ionic rectification in a 10 mM KCl solution at different pH values. (a) *I–V* curves of the AAO-PVA/WO_3 nanochannels measured at pH 3, pH 7, and pH 11. (b) Histogram of the rectification ratios calculated from the *I–V* curves.

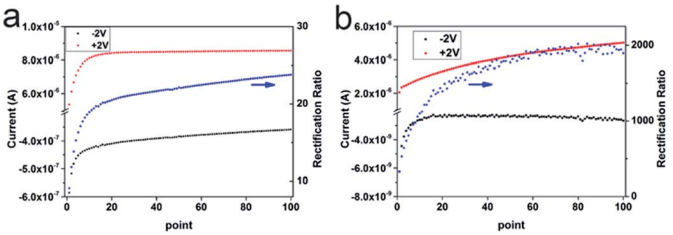

Fig. 4 Characterization of the ion current and the corresponding rectification ratio in a 10 mM KCl solution at constant voltage. The red and black squares represent the ion current at +2 V and −2 V, respectively, and the blue represent the corresponding rectification ratios. (a) PVA modified hourglass-shaped AAO. (b) PVA/WO_3 covered hourglass-shaped AAO.

Open Access Article. Published on 18 February 2020. Downloaded on 1/20/2026 11:38:05 AM.
This article is licensed under a Creative Commons Attribution-NonCommercial 3.0 Unported Licence.

Conclusions

We have successfully prepared thin nanoporous PVA/WO_3 covered hourglass-shaped AAO nanochannels using the facile spin coating method. The preparation method combines the advantages of the nanochannels and provides a stronger nano-confined effect. The nanoporous thin coating greatly reduced the opening size of the AAO nanochannels, forming an "ion pool" with one end. There is a homogenous junction in the middle of the hourglass-shaped AAO, while the other end has a heterogeneous structure. The PVA/WO_3 covered hourglass-shaped nanochannels display an extremely high rectifying performance in neutral KCl solution, which comes from ion enrichment and ion depletion of the "ion pool". The rectifying effect performance is greatly enhanced under constant voltage due to cooperative effects between the two small open ends and the long dimensionality of the "ion pool". The rectifying effect is sensitive to the pH value of the electrolyte solution and a single rectification direction is activated from acidic to basic conditions. This simple preparation method and nano-confined strategy can be extended to other material fields.

Conflicts of interest

There are no conflicts to declare.

Acknowledgements

This work was supported by the National Key Research and Development Program of China (2017YFA0206902, 2017YFA0206900), and the National Natural Science Foundation of China (21975009, 21641006, 21701159).

Notes and references

1 E. Gouaux and R. MacKinnon, *Science*, 2005, **310**, 1461–1465.
2 E. García-Giménez, A. Alcaraz, V. M. Aguilella and P. Ramírez, *J. Membr. Sci.*, 2009, **331**, 137–142.
3 S. Chen, Y. Tang, K. Zhan, D. Sun and X. Hou, *Nano Today*, 2018, **20**, 84–100.
4 Y. Zhu, K. Zhan and X. Hou, *ACS Nano*, 2018, **12**, 908–911.
5 Y. Tang, L. Cao, K. Zhan, Y. Xie, D. Sun, X. Hou and S. Chen, *Sens. Actuators, B*, 2019, **286**, 315–320.
6 Q. Ma, Z. Si, Y. Li, D. Wang, X. Wu, P. Gao and F. Xia, *TrAC, Trends Anal. Chem.*, 2019, **115**, 174–186.
7 Z. Siwy and A. Fuliński, *Phys. Rev. Lett.*, 2002, **89**, 198103.
8 Y. Sun, J. Ma, F. Zhang, F. Zhu, Y. Mei, L. Liu, D. Tian and H. Li, *Nat. Commun.*, 2017, **8**, 260.
9 C. Li, F. Ma, Z. Wu, H. Gao, W. Shao, K. Wang and X. Xia, *Adv. Funct. Mater.*, 2013, **23**, 3836–3844.
10 S. Wu, F. Wildhaber, A. Bertsch, J. Brugger and P. Renaud, *Appl. Phys. Lett.*, 2013, **102**, 213108.
11 Z. Wang, X. Fan, Q. Wang, S. Hou, H. Wang, J. Zhai and X. Meng, *RSC Adv.*, 2016, **6**, 63652–63659.
12 Y. Liu, Y. Kong, X. Fan, J. Zhai and L. Jiang, *J. Mater. Chem. A*, 2017, **5**, 19220.
13 L. J. Cheng and L. J. Guo, *Nano Lett.*, 2007, **7**, 3165–3171.
14 R. Karnik, C. Duan, K. Castelino, H. Daiguji and A. Majumdar, *Nano Lett.*, 2007, **7**, 547–551.
15 J. Zhang, Y. Yang, Z. Zhang, P. Wang and X. Wang, *Adv. Mater.*, 2014, **26**, 1071–1075.
16 S. Z. Siwy, *Adv. Funct. Mater.*, 2006, **16**, 735–746.
17 I. Vlassiouk and S. Z. Siwy, *Nano Lett.*, 2007, **7**, 552–556.
18 I. Vlassiouk, S. Smirnov and Z. Siwy, Nanofluidic ionic diodes, *ACS Nano*, 2008, **2**, 1589–1602.
19 Y. Jiang, A. Lee, J. Chen, V. Ruta, M. Cadene, B. T. Chait and R. MacKinnon, *Nature*, 2003, **423**, 33–41.
20 Y. Lei, F. Xie, W. Wang, W. Wu and Z. Li, *Lab Chip*, 2010, **10**, 2338–2340.
21 I. Zharov and A. Khabibullin, *Acc. Chem. Res.*, 2014, **47**, 440–449.
22 E. Choi, C. Wang, G. T. Chang and J. Park, *Nano Lett.*, 2016, **16**, 2189–2197.
23 M. Wang, H. Meng, D. Wang, Y. Yin, P. Stroeve, Y. Zhang, Z. Sheng, B. Chen, K. Zhan and X. Hou, *Adv. Mater.*, 2019, **31**, 1805130.
24 E. Barry, S. P. McBride, H. M. Jaeger and X. M. Lin, *Nat. Commun.*, 2014, **5**, 5847.
25 D. G. Haywood, A. Saha-Shah, L. A. Baker and S. C. Jacobson, *Anal. Chem.*, 2015, **87**, 172–187.
26 J. Gao, W. Guo, D. Feng, H. Wang, D. Zhao and L. Jiang, *J. Am. Chem. Soc.*, 2014, **136**, 12265–12272.
27 Q. Zhang, Z. Hu, Z. Liu, J. Zhai and L. Jiang, *Adv. Funct. Mater.*, 2014, **24**, 424–431.
28 X. Sui, Z. Zhang, Z. Y. Zhang, Z. Wang, C. Li, H. Yuan, L. Gao, L. Wen, X. Fan, L. Yang, X. Zhang and L. Jiang, *Angew. Chem., Int. Ed.*, 2016, **55**, 13056–13060.
29 Z. Zhang, X. Y. Kong, K. Xiao, G. Xie, Q. Liu, Y. Tian, H. Zhang, J. Ma, L. Wen and L. Jiang, *Adv. Mater.*, 2016, **28**, 144–150.
30 S. Rao, K. J. Si, L. W. Yap, Y. Xiang and W. Cheng, *ACS Nano*, 2015, **9**, 11218–11224.
31 K. Han, L. Heng, L. Wen and L. Jiang, *Nanoscale*, 2016, **8**, 12318–12323.
32 H. Wang, Q. Liu, W. Li, L. Wen, D. Zheng, Z. Bo and L. Jiang, *ACS Nano*, 2016, **10**, 3606–3613.
33 W. Guo, Y. Tian and L. Jiang, *Acc. Chem. Res.*, 2013, **46**, 2834–2846.
34 D. Zhang, Q. Q. Wang, X. Fan, M. L. Zhang, J. Zhai and L. Jiang, *Adv. Mater.*, 2018, **30**, 1804862.
35 S. Umehara, N. Pourmand, C. D. Webb, R. W. Davis, K. Yasuda and M. Karhanek, *Nano Lett.*, 2006, **6**, 2486–2492.
36 L. J. Cheng and L. J. Guo, *ACS Nano*, 2009, **3**, 575–584.
37 Z. S. Siwy and S. Howorka, *Chem. Soc. Rev.*, 2010, **39**, 1115–1132.
38 X. Hou, H. Zhang and L. Jiang, *Angew. Chem., Int. Ed.*, 2012, **51**, 5296–5307.
39 J. Cervera, A. Alcaraz, B. Schiedt, R. Neumann and P. Ramírez, *J. Phys. Chem. C*, 2007, **111**, 12265–12273.
40 B. Yameen, M. Ali, R. Neumann, W. Ensinger, W. Knoll and O. Azzaroni, *J. Am. Chem. Soc.*, 2009, **131**, 2070–2071.
41 Z. S. Siwy, E. Heins, C. C. Harrell, P. Kohli and C. R. Martin, *J. Am. Chem. Soc.*, 2004, **126**, 10850–10851.

 This journal is © The Royal Society of Chemistry 2020

Open Access Article. Published on 18 February 2020. Downloaded on 1/20/2026 11:38:05 AM.
This article is licensed under a Creative Commons Attribution-NonCommercial 3.0 Unported Licence.

42 E. B. Kalman, I. Vlassiouk and Z. S. Siwy, *Adv. Mater.*, 2008, **20**, 293–297.
43 X. Hou, Y. Liu, H. Dong, F. Yang, N. Li and L. Jiang, *Adv. Mater.*, 2010, **22**, 2440–2443.
44 M. Ali, P. Ramirez, H. Q. Nguyen, S. Nasir, J. Cervera, S. Mafe and W. Ensinger, *ACS Nano*, 2012, **6**, 3631–3640.
45 M. Zhang, X. Hou, J. Wang, Y. Tian, X. Fan, J. Zhai and L. Jiang, *Adv. Mater.*, 2012, **24**, 2424–2428.
46 H. Zhang, X. Hou, L. Zeng, F. Yang, L. Li, D. Yan, Y. Tian and L. Jiang, *J. Am. Chem. Soc.*, 2013, **135**, 16102–16110.
47 H. Daiguji, Y. Oka and K. Shirono, *Nano Lett.*, 2005, **5**, 2274–2280.
48 R. Fan, S. Huh, R. Yan, J. Arnold and P. Yang, *Nat. Mater.*, 2008, **7**, 303–307.
49 R. Yan, W. Liang, R. Fan and P. Yang, *Nano Lett.*, 2009, **9**, 3820–3825.
50 H. Miedema, M. Vrouenraets, J. Wierenga, W. Meijberg, G. Robillard and B. Eisenberg, *Nano Lett.*, 2007, **7**, 2886–2891.
51 K. Raidongia and J. Huang, *J. Am. Chem. Soc.*, 2012, **134**, 16528–16531.
52 J. J. Shao, K. Raidongia, A. R. Koltonow and J. Huang, *Nat. Commun.*, 2015, **6**, 7602.
53 T. Xiao, Q. Liu, Q. Zhang, Z. Liu and J. Zhai, *J. Phys. Chem. C*, 2017, **121**, 18954–18961.
54 B. Bao, J. Hao, X. Bian, X. Zhu, K. Xiao, J. Liao, J. Zhou, Y. Zhou and L. Jiang, *Adv. Mater.*, 2017, **29**, 1702926.
55 L. Lin, J. Yan and J. Li, *Anal. Chem.*, 2014, **86**, 10546–10551.
56 E. Madrid, Y. Rong, M. Carta, N. B. McKeown, R. Malpass-Evans, G. A. Attard, T. J. Clarke, S. H. Taylor, Y. T. Long and F. Marken, *Angew. Chem., Int. Ed.*, 2014, **126**, 10927–10930.
57 L. H. Yeh, M. Zhang and S. Qian, *Anal. Chem.*, 2013, **85**, 7527–7534.
58 R. T. Perera, R. P. Johnson, M. A. Edwards and H. S. White, *J. Phys. Chem. C*, 2015, **119**, 24299–24306.
59 Q. Zhang, Z. Liu, K. Wang and J. Zhai, *Adv. Funct. Mater.*, 2015, **25**, 2091–2098.